ACS Energy LETTERS

http://pubs.acs.org/journal/aelccp

Correlating the Formation Protocols of Solid Electrolyte Interphases with Practical Performance Metrics in Lithium Metal Batteries

Solomon T. Oyakhire, Wenbo Zhang, Zhiao Yu, Sarah E. Holmes, Philaphon Sayavong, Sang Cheol Kim, David T. Boyle, Mun Sek Kim, Zewen Zhang, Yi Cui,* and Stacey F. Bent*

Cite This: *ACS Energy Lett.* 2023, 8, 869–877

Read Online

ACCESS | Metrics & More | Article Recommendations | Supporting Information

ABSTRACT: **The solid electrolyte interphase (SEI) is regarded as the most important and least understood component of lithium metal batteries (LMBs). Similarly, the connection between SEI formation protocols and the practical performance metrics in LMBs is even less understood. Here, we demonstrate the effects of constant current and constant voltage SEI formation protocols on Coulombic efficiency (CE) and corrosion losses in LMBs. The formation protocols produce SEIs that reduce parasitic lithium−electrolyte reactions, improving early cycle CE and mitigating corrosion of lithium metal. In addition, we establish that the thicker constant current SEIs formed at low current densities are better for passivating lithium than constant voltage SEIs, possibly due to reduced electrolyte permeability in the constant current SEIs. Using these SEI formation protocols in a high-performing electrolyte, we improve first-cycle CE by ∼5%, improve compounded CE in the first 5 cycles by ∼7%, and reduce corrosion-induced CE losses by ∼8%.**

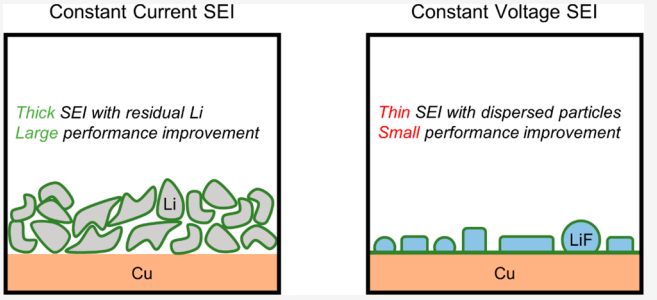

The electrification of the transportation sector is crucial for enabling a renewable energy future.[1] However, one obstacle to the deployment of electric vehicles is the design of reliable high energy density batteries.[2] One of the most promising energy storage technologies is the lithium metal battery (LMB). It is regarded as the holy grail of energy storage due to the low redox potential (−3.04 V vs standard hydrogen electrode) and high gravimetric capacity (3860 mAh g^{-1}) of lithium.[3−5] Unfortunately, lithium metal is plagued by numerous parasitic reactions that forestall its deployment. These reactions involve the continuous consumption of lithium during battery operation, resulting in low Coulombic efficiency (CE) and poor cycle life of LMBs.[3−6]

Electrolyte engineering is becoming the premier strategy for improving CE and cycle life in LMBs.[7−11] Most electrolyte engineering strategies involve the modulation of chemical species within the electrolyte mixture with an aim of forming a stable interphase between lithium and the electrolyte.[7,8,12] This interphase, known as the solid electrolyte interphase (SEI), acts as a solid barrier that prevents lithium metal from reacting further with the electrolyte. Studies have shown that the control and design of the SEI can be achieved by using additives,[13−15] modifying solvent molecules,[7,11,16] and changing the chemical speciation of lithium salts.[9,12,13,17] These changes in electrolyte speciation have informed the design of one promising class of high-performing electrolytes—weakly solvating electrolytes.[18−22] In weakly solvating electrolytes, the mixture of solvent and salt is designed such that there is preferential decomposition of anions, resulting in the formation of favorable SEI species. Besides the likelihood of forming favorable SEIs, the number of electrochemical cycles required for the SEI to passivate lithium metal is also crucial, as it determines available battery capacity. The quickness of lithium passivation dictates some of the practical performance metrics in a battery, such as the first-cycle CE, the compounded CE over the first few cycles, and the extent of

Received: September 20, 2022
Accepted: December 19, 2022

https://doi.org/10.1021/acsenergylett.2c02137
ACS Energy Lett. 2023, 8, 869–877

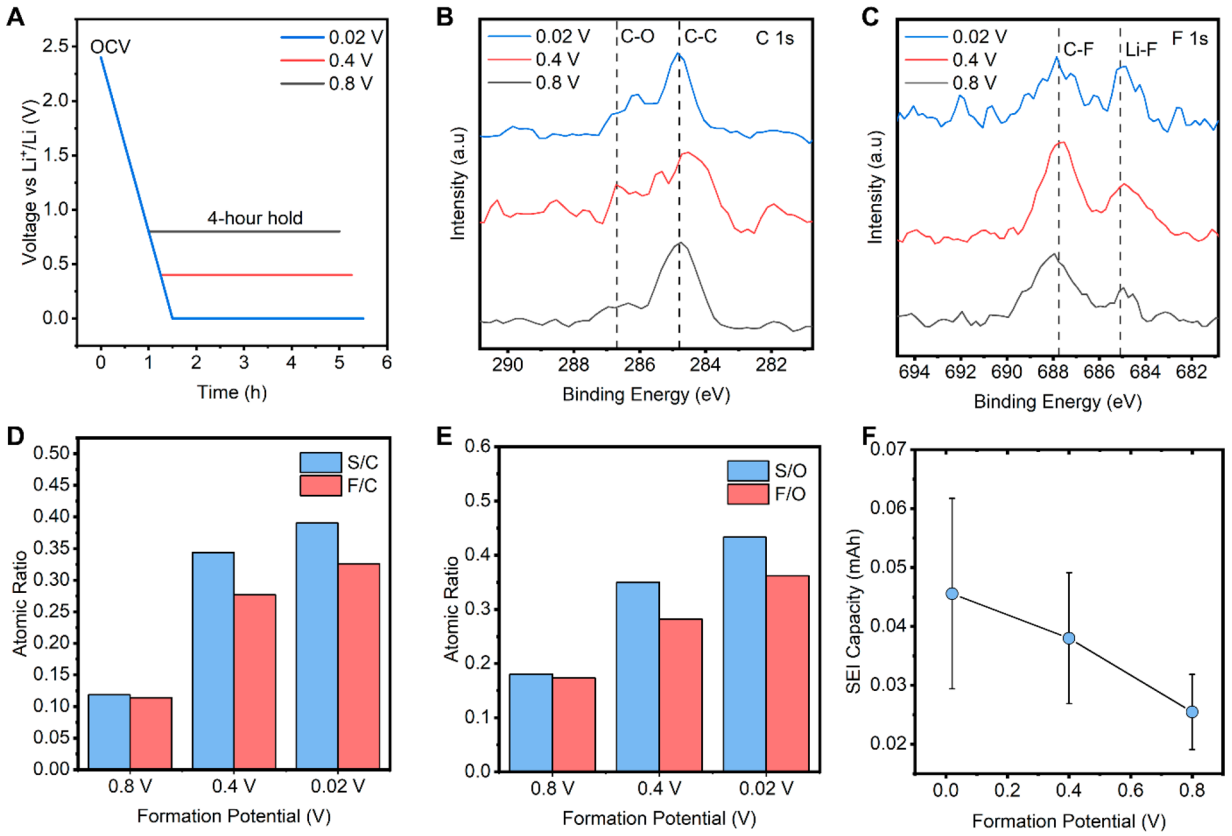

Figure 1. Constant voltage protocols result in SEI formation. A. Illustration of the SEI formation concept at the potentials used in this study. Cells are slowly charged (at 50 μA/cm^2) from OCV to the corresponding potentials and held at those potentials for 4 h. B, C. XPS high-resolution profiles of SEIs formed at different potentials showing the C 1s and F 1s spectra, respectively. D. Atomic ratio of S/C and F/C in SEIs formed at different potentials, derived from XPS. E. Atomic ratio of S/O and F/O in SEIs formed at different potentials, derived from XPS. F. SEI capacity as a function of formation potential. Error bars represent one standard deviation.

corrosion loss in a battery.[23−25] One method for improving lithium passivation is the design of SEI formation protocols, and while a few studies have focused on understanding how the SEI changes under different protocols,[26,27] no report has proposed a clear connection between SEI formation protocols and practical performance metrics in LMBs. To design better performing LMBs, it is important to understand how SEI formation impacts lithium passivation and, in turn, the practical performance metrics of LMBs.

In this work, we design constant voltage and constant current protocols for forming SEIs using a high-performing weakly solvating electrolyte, 1 M lithium bis(fluorosulfonyl)-imide salt in fluorinated 1,4-dimethoxylbutane solvent (1 M LiFSI/FDMB),[7] then we draw connections between the SEIs and performance metrics of LMBs. The constant voltage protocols result in Li metal-free SEIs, while the constant current protocols promote Li metal-containing SEIs, providing two templates to examine the impact of SEI on LMB performance. In the constant voltage protocols, we vary the potential at which the cell is held during SEI formation, and in the constant current protocols, we vary the current density at which the cell is cycled during SEI formation. Both protocols form SEIs that improve CE and reduce corrosion, and the extent of their improvement depends on the nature of the SEIs. Under the constant voltage protocols, lower potentials improve performance metrics by enabling the formation of anion-rich SEIs, while during the constant current protocols, lower current densities enable the formation of thicker SEIs that reduce parasitic side reactions between Li and the electrolyte. The electrolyte used in this study, 1 M LiFSI/FDMB, is a high-performing state-of-the-art electrolyte,[7] making its performance improvements relevant for enabling practical LMBs.

SEI Formation Using Constant Voltage. One of the most common ways to prepare the SEI is with a constant voltage protocol.[26,27] The constant voltage SEI formation protocols used in this study were carried out in LillCu cells. Cells were slowly discharged from open-circuit voltage (OCV) at a current density of 50 μAcm^{-2} and affixed at 0.8, 0.4, or 0.02 V vs Li$^+$/Li for 4 h (Figure 1A). By fixing cells at potentials below 1 V and above 0 V, we ensure decomposition of salt and solvent but avoid lithium deposition, which does not occur until voltages below 0 V.[26−28] These conditions provide a template for understanding how SEI formation prior to lithium deposition impacts the performance of LMBs.

One aspect to consider when assessing the SEI is its chemical composition. X-ray photoelectron spectroscopy (XPS) results, collected using protocols consistent with recent guidelines,[29] show the SEI chemical composition in the 1 M LiFSI/FDMB electrolyte across all constant voltage formation conditions (Figure 1B,C). LiFSI contains N, S, O, F, and Li, while FDMB contains C, O, and F, so C is a unique solvent decomposition signature while N and S represent unique anion decomposition signatures. From the high-resolution XPS spectra for all SEIs, C−C and C−O species are formed (Figure 1B), and they are attributed to the decomposition of the FDMB solvent. XPS also reveals decomposed fluorine-

https://doi.org/10.1021/acsenergylett.2c02137
ACS Energy Lett. 2023, 8, 869−877

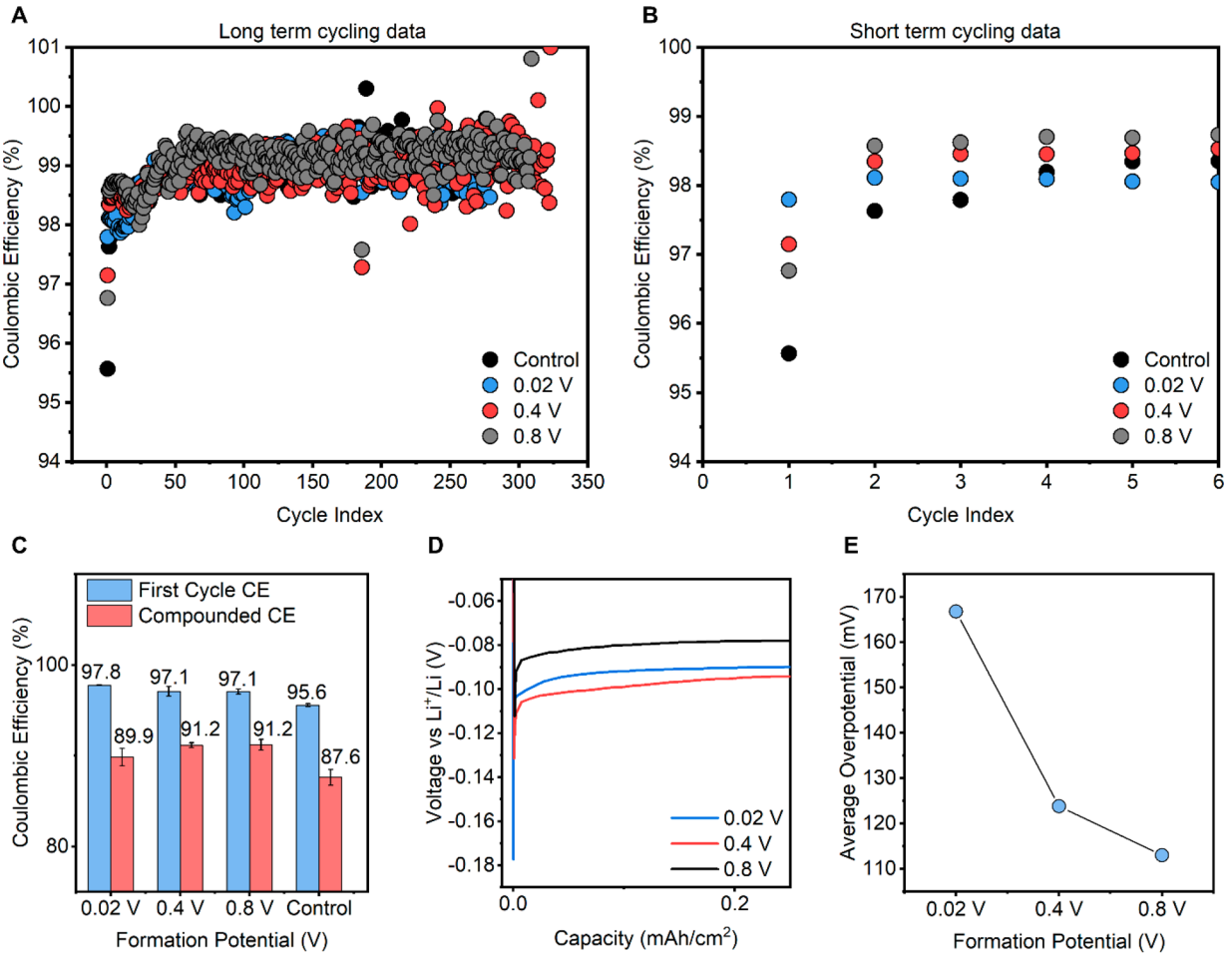

Figure 2. Constant voltage SEIs improve CE of Li||Cu cells. A, B. CE results of Li||Cu cells cycled over long and short terms, respectively at 1 mA/cm^2 and 1 mAh/cm^2 for various formation conditions, for one representative cell in each formation protocol. C. First-cycle CE and compounded CE after 5 cycles at 1 mA/cm^2, as a function of formation potential, averaged over three cells. Error bars represent one standard deviation. D. First-cycle voltage profiles for Li||Cu cells cycled at 1 mA/cm^2, as a function of formation potential, for one representative cell in each formation protocol. E. Average first-cycle overpotential as a function of formation potential averaged over at least two Li||Cu cells cycled at 1 mA/cm^2.

containing compounds such as C−F and Li−F (Figure 1C). In addition, there is an increase in the Li−F peak intensity compared to that of C−F as formation potential decreases, suggesting a decrease in the likelihood for solvent decomposition relative to anion decomposition at lower formation potentials, since the anion is carbon-free. Many studies have shown that anion-rich SEIs provide better passivation (formation of a reaction-minimizing interphase) over lithium metal,[7,18,20] so we investigate the likelihood of anion decomposition at lower potentials by examining elemental ratios retrieved from XPS. The electrolyte anion (FSI^-) is the only sulfur-containing species and the electrolyte solvent (FDMB) is the only carbon-containing species, so the S/C ratio indicates the likelihood of anion-to-solvent decomposition. As formation potential decreases, the S/C ratio increases, suggesting an increasing preference for anion decomposition (Figure 1D). Similarly, the F/C ratio increases as the formation potential decreases, and because we have established that anion decomposition becomes favored at lower potentials, the F/C increase suggests that the fluorine contributions from anion decomposition increase with decreasing potential (Figure 1D). These findings are consistent with the increase in Li−F formation shown in Figure 1C. The ratios of S/O and F/O also present similar trends, with a decrease in formation potential leading to an increase in S/O and F/O (Figure 1E). This trend in preferential anion decomposition is also verified across three distinct spatial locations atop the SEIs (Figure S1). Taken together, the XPS results indicate that as potential is reduced in our system, anion decomposition becomes preferred over solvent decomposition. The increase in anion decomposition at lower potentials is likely due to a local enrichment of anions at the current collector surface.

While XPS provides details of the chemical species in the SEI, it is also important to understand the kinetics of electrolyte decomposition during the constant voltage formation conditions. To understand the kinetics, we investigate SEI capacity (defined here as the quantity of charge passed during electrolyte decomposition and calculated as the integral of current over time during SEI formation conditions) using coulometry. As formation potential decreases, SEI capacity increases (Figure 1F). This increase in SEI capacity with a decrease in formation potential could be due to differences between OCV and formation potentials: since the cells are discharged at the same current density, additional time is required to attain lower potentials, resulting in an increase in SEI capacity at lower potentials. In addition,

https://doi.org/10.1021/acsenergylett.2c02137
ACS Energy Lett. 2023, 8, 869−877

current decay trends during the formation process indicate that the kinetics of electrolyte decomposition is accelerated at lower potentials (Figure S2). Combined, the data suggest that as potential is lowered during formation, both the quantity of SEI formed and the preference for anion decomposition increase. This finding is important because several studies have postulated that anion-rich and thicker SEIs are better for LMB performance.[7,18]

Effects of Constant Voltage SEIs on Coulombic Efficiency. To understand how constant voltage formation protocols impact performance, we measure CE using Li||Cu cells cycled at 1 mA/cm^2 with a capacity of 1 mAh/cm^2. The data show that SEIs derived from constant voltage do not significantly impact the long-term cycle life of Li||Cu, since the control cell and cells with constant voltage SEI all last until at least 300 cycles (Figure 2A). This similarity in long-term performance is likely due to the passivation of lithium metal in the FDMB electrolyte over long-term cycling, so all cells, regardless of the preformation protocol, end up converging to the same performance over long-term cycling.[7] On the other hand, short-term performance metrics show differences. Even though long-term performance stability is desired of LMBs, the practical deployment of LMBs will also be dependent on short-term metrics such as first-cycle CE and compounded CE over the first few cycles. Specifically, the premier architecture of LMBs, anode-free cells,[9] requires high first-cycle CE and compounded CE, since early losses in CE reduce the available capacity in anode-free LMBs. To that end, we investigate the benefits of the constant voltage SEIs on first-cycle and compounded CE. The formation conditions cause notable changes in the average first-cycle CE of the cells, with a value of 95.6% for the control cell, 97.1% for the 0.4 and 0.8 V cells, and 97.8% for the 0.02 V cells (Figure 2B,C). This result suggests that the SEIs identified in Figure 1 reduce lithium−electrolyte reactions in the first cycle, resulting in higher first-cycle CE. Specifically, as formation potential is lowered, first-cycle CE increases, suggesting that the increase in SEI capacity and SEI inorganic content improves lithium passivation. To verify that the improvements in first-cycle CE are due to better lithium passivation rather than reversible SEI capacity, we form the SEI at 0.02 V and quantify the extent of its reversibility under oxidative conditions (Figure S3). Since only 0.3% of the formed SEI capacity is recovered during oxidation, changes in first-cycle CE can be attributed to better lithium passivation at lower potentials. The convergence of CEs after the first cycle in Figure 2B shows that other sources of capacity loss begin to dominate SEI losses as cycle number increases, consistent with recent studies that attribute CE losses after early cycling stages to the electrical isolation of lithium.[30,31]

We also look at a parameter called compounded CE to better capture the cell behavior over multiple cycles. Compounded CE across the first 5 cycles is calculated using eq 1:

$$\text{Compounded CE} = 100 \times \prod_{i=1}^{5} f_{\text{CE}_i} \tag{1}$$

where f_{CE_i} is the fractional CE in each battery cycle, i.

The compounded CE across the first 5 cycles also reveals benefits of constant voltage formation conditions (Figure 2C). The average compounded CE after the first 5 cycles is 87.6% for the control cell, while the compounded CEs for the 0.8, 0.4, and 0.02 V cells are 91.2%, 91.2%, and 89.9%, respectively. These differences in compounded CE can be attributed to the early stage stability in lithium plating and stripping that is conferred by the preformed SEI. We note that the differences in compounded efficiencies are not as significant as the differences in first-cycle CE because of how quickly this electrolyte forms a stable passivation layer. We analyze the voltage curve in the first cycle of Li deposition to further understand the improvements conferred by the constant voltage SEI. First-cycle discharge voltage curves reveal that overpotential increases as formation potential is lowered (Figure 2D,E). Here, overpotential is defined as the inflection point (lowest point) on the voltage curves shown in Figure 2D, as it reflects the energy barrier that must be surpassed before nucleation of lithium occurs. For the 0.8, 0.4, and 0.02 V cells, the average overpotential for at least two cells each is 113 mV, 123.9 mV, and 166.8 mV, respectively (Figure 2D,E). These changes in overpotential are consistent with the SEI capacity and chemistry shown in Figure 1D−F: as SEI capacity increases and as the SEI becomes richer in anions, overpotential increases. This correlation in turn suggests that as the quantities of SEI formed (charges consumed) and SEI anionic components increase, the SEI becomes more resistive to ion transport, resulting in higher overpotential. The increase in first-cycle overpotential is also consistent with the first-cycle CE trend observed in Figure 2C: as the SEI capacity increases, the first-cycle CE increases. To decouple the effects of SEI chemistry from SEI capacity, we vary the SEI formation duration at 0.02 V and observe that when SEI capacity increases and SEI chemistry remains similar, there is no significant change in CE (Figure S4). This result suggests that the increase in CE across the formation potentials can mostly be attributed to the change in SEI chemistry.

To verify that the improvements in early cycle performance of the cells are caused by the formed SEIs, we examine the morphology of lithium deposited after constant voltage formation and control conditions. The morphology of lithium indicates lithium−electrolyte contact area and how much reaction occurs between lithium and the electrolyte.[32,33] Between the constant voltage formation and control conditions, there is no noticeable difference in the deposition morphology of lithium in the first cycle of lithium plating (Figure S5). Similar lithium morphology connotes similar contact area between lithium and the electrolyte. Hence, the improvements in first-cycle and compounded CE are most likely caused by the improved lithium passivation of the constant voltage SEIs rather than lithium morphology changes. It is noteworthy that a recent study reported that performance improves at higher SEI formation potentials.[34] However, we hypothesize that the difference in performance trends between our study and theirs originates from differences in electrolyte solvation and decomposition kinetics, making our electrolyte more likely to form better passivating SEIs at lower potentials, while their electrolyte forms better passivating SEIs at higher potentials.

Effects of Constant Current SEIs on Coulombic Efficiency. Another method for forming the SEI involves cycling the battery under constant current protocols. This method promotes the formation of Li metal-containing SEI[35] unlike the constant voltage protocols, providing a different template for understanding SEI formation. The constant current formation cycles adopted in this study were carried out in Li||Cu cells. We note that the constant current protocols are unavoidably carried out at different voltages, so it is

https://doi.org/10.1021/acsenergylett.2c02137
ACS Energy Lett. 2023, 8, 869−877

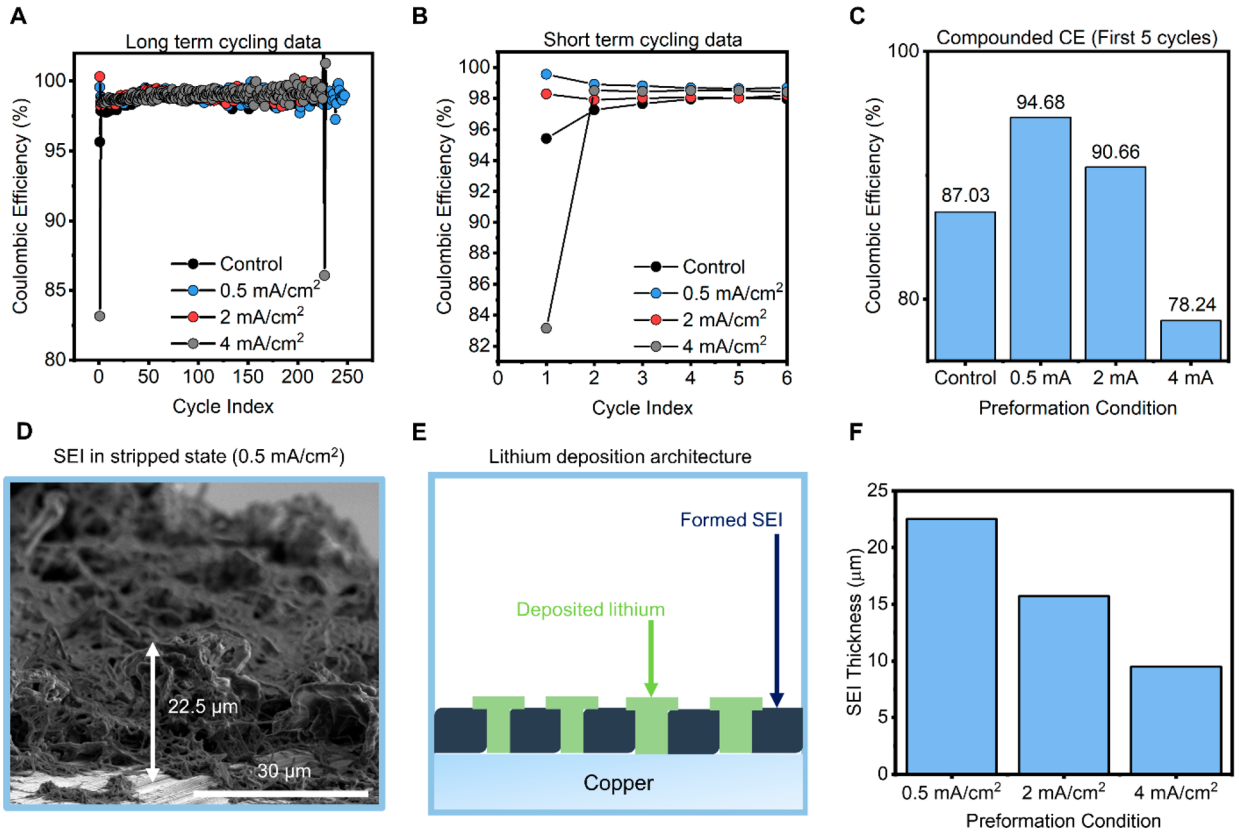

Figure 3. Constant current SEIs improve CE in Li||Cu cells. A,B. Long and short-term cycling results, respectively, of Li||Cu cells cycled at 1 mA/cm^2 and 1 mAh/cm^2 after various constant current conditions. C. Compounded CE of cells in panel B in the first 5 electrochemical cycles with reported currents normalized to an active electrode area of 1 cm^2. D. Cross-sectional view by SEM of SEI formed atop copper after 10 cycles of plating and stripping 0.5 mAh/cm^2 of lithium at 0.5 mA/cm^2. E. Illustration of lithium plating within the constant current SEI. F. SEI thickness for each corresponding preformation condition.

challenging to fully decouple the effects of voltage from the constant current protocols. We form the SEI by cycling 0.5 mAh/cm^2 of lithium at 0.5 mA/cm^2, 2 mA/cm^2, and 4 mA/cm^2, for 10 cycles. Subsequently, we investigate how the SEI formed at those current densities impacts the performance of Li||Cu cells cycled at 1 mA/cm^2 with a capacity of 1 mAh/cm^2. The data show that formation conditions with this constant current protocol do not significantly affect the long-term cycling of Li||Cu cells (Figure 3A). This similarity in long-term cycle life is expected because the FDMB electrolyte forms a self-passivating SEI after repeated lithium deposition cycles.[7] However, in the early stages of cycling, where the practicality of battery technologies is determined, formation protocols result in different first-cycle CEs of 94.8%, 99.5%, 98.1%, and 82.5%, for the control, 0.5 mA/cm^2, 2 mA/cm^2, and 4 mA/cm^2 cells, respectively (Figure 3B,C). In addition, compounded CEs within the first 5 cycles are 87.03%, 94.88%, 90.66%, and 78.24% for the control, 0.5 mA/cm^2, 2 mA/cm^2, and 4 mA/cm^2 cells, respectively (Figure 3C). The results show improved CE in cells cycled at lower current densities (0.5 mA/cm^2 and 2 mA/cm^2) and worse CE in cells cycled at 4 mA/cm^2, suggesting that the preformed SEI affects parasitic reactions of lithium metal in the early stages of electrodeposition and that this effect is dependent on current density. These differences in CE indicate the importance of formation conditions in the cycling of LMBs. Similar results are observed in replicate cells, showing that the findings are reproducible (Figure S6).

To understand why constant current SEI formation impacts performance, we perform SEM analysis on the SEI formed at 0.5 mA/cm^2. As shown in Figure 3D, a network of SEI species is formed on the current collector after the 0.5 mA/cm^2 formation protocol. According to SEM-EDS (Figure S7), this network of SEI species contains a uniform distribution of S, F, and C, the elements that are expected during the decomposition of 1 M LiFSI/FDMB.[7] To understand how this SEI network impacts lithium electrodeposition, we deposit 1 mAh/cm^2 of lithium on the SEI formed at 0.5 mA/cm^2. Notably, there is no lithium observed via the cross-sectional SEM image (Figure S8A), while there are lithium deposits observed in the plan view SEM images (Figure S8B), suggesting that lithium deposits within the pores of the SEI structure, from the base of the SEI upward. This deposition configuration is similar to that in the report by Wang et al. in which they refer to the SEI as residual SEI.[35] As such, we propose that the deposited lithium grows within the pores of the SEI structure, as illustrated in Figure 3E. This morphology, in which the SEI poses a barrier between Li and the electrolyte, suggests that the SEI acts as a pseudohost that reduces reactions between deposited lithium and the electrolyte. With this proposed mode of SEI passivation, the benefits of this SEI are likely dependent on its structure. Using cross sectional SEM, we investigate the thickness of SEIs formed at different formation conditions. The thickness of the SEIs decreases with increasing current density (22.5 μm, 15.71 μm, and 9.46 μm for the 0.5 mA/cm^2, 2 mA/cm^2, and the 4 mA/cm^2 protocols,

https://doi.org/10.1021/acsenergylett.2c02137
ACS Energy Lett. 2023, 8, 869−877

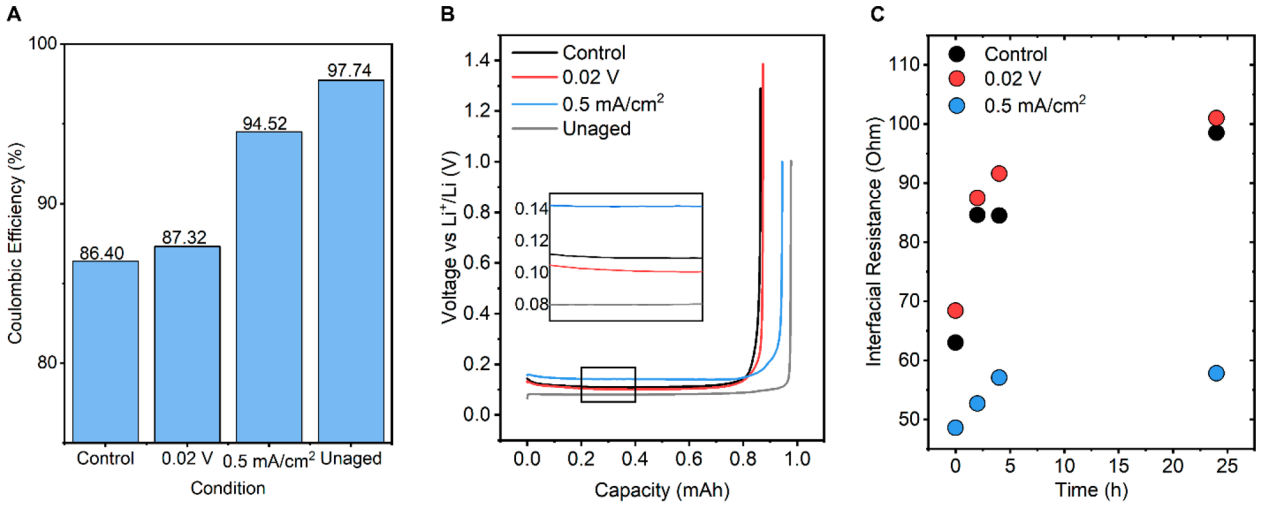

Figure 4. SEI formation strategies reduce corrosion-derived capacity losses. A. Coulombic efficiency of Li−Cu cells after 24 h of aging. B. Voltage profiles for the aged cells in panel A during lithium stripping at 1 mA/cm^2. C. Interfacial resistance as a function of aging time for different formation conditions, determined from EIS measurements.

respectively) as shown in Figures 3D and S8C,D, possibly because lithium deposition morphology becomes thinner and more heterogeneous as current density increases, resulting in thinner SEI shells. In addition, the quantity of lithium consumed during SEI formation increases with increasing current density (0.14 mAh, 0.16 mAh, and 0.23 mAh, for the 0.5 mA/cm^2, 2 mA/cm^2, and the 4 mA/cm^2 protocols, respectively) as shown in Figure S9. The correlation between SEI thickness and lithium consumed during SEI formation suggests that the SEI structures differ in porosity, with the 0.5 mA/cm^2 SEI possessing the most porous structure and the 4 mA/cm^2 SEI possessing the least porous structure. This correlation is consistent with the mode of Li growth that we propose in Figure 3G. We hypothesize that for thicker and more porous SEI structures, lithium nucleates within the pores of the SEI and remains passivated when growing in the upward direction, explaining the increase in CE with decreasing current density. Our hypothesis is supported by SEM images, which reveal the poorer passivation of Li deposited within the 2 mA/cm^2 and 4 mA/cm^2 SEI structures (Figure S10). Using XPS, we also show that the SEIs formed at all current densities are chemically similar (Figure S11), suggesting that the changes in CE are caused by differences in SEI thicknesses and porosities and not by differences in the chemical composition of the SEI.

Effects of SEI Formation on Corrosion Losses in Lithium Metal Batteries. Corrosion is an underexplored but important pathway for capacity loss in LMBs, and is determined by the passivity of the SEI.[23−25,31] To examine how our SEI formation strategies affect the rate of corrosion, we age (rest at open-circuit voltage) for 24 h 1 mAh/cm^2 lithium deposited in the second electrochemical cycle, then examine the extent of lithium corrosion by using CE to quantify lithium recoverability after aging. The CE after aging reflects the quantity of lithium that is electrochemically available. We examine the effects of aging on the control cell, the 0.5 mA/cm^2 constant current SEI cell, and the 0.02 V constant voltage SEI cell to compare how aging varies with SEI formation protocols. As shown in Figure 4A, the cells display different CEs depending on formation protocols. In comparison to the unaged cell which has a CE of 97.74% in the second cycle, the control cell which is aged without SEI preformation has a CE of 84.60%. On the other hand, cells with SEI formed at 0.02 V and 0.5 mA/cm^2 display improved CEs of 87.32% and 94.52%, respectively, after aging. This trend in CE after corrosion is verified using three cell replicates, as shown in Figure S12. The CE losses after aging in the second cycle are likely caused by SEI growth, as demonstrated by Boyle et al.[25] These SEI-mediated CE losses are caused by continuous reactions between lithium and the electrolyte during resting, resulting in loss of electrochemically active lithium to SEI formation. Our CE results in Figure 4A, taken together with this mechanism of SEI-mediated corrosion, suggest that the thick SEI formed at 0.5 mA/cm^2 reduces reactions between lithium and the electrolyte by reducing electrolyte penetration into the electrodeposited lithium. It is noteworthy that we used a large quantity of electrolyte (60 μL) to prevent electrolyte quantity-dependent corrosion rates between our formation processes and the control cell. Also, because the 0.02 V protocol is expected to reduce galvanic corrosion,[24] it is reasonable to attribute most of the observed CE losses to chemical corrosion.

Voltage profiles also provide additional insights into the effects of aging on electrodeposited lithium across our cells. After aging lithium, the voltage profiles shown in Figure 4B reveal that the cell with 0.5 mA/cm^2 SEI has the highest steady-state overpotential (0.14 V), indicating that the 0.5 mA/cm^2 SEI framework is resistive to lithium-ion transport. Similar trends are observed prior to aging, in which the 0.5 mA/cm^2 cell has a steady-state overpotential that is 50 mV higher than those of the control and 0.02 V cells (Figure S13). This suggests that the reduction in corrosion losses observed in the 0.5 mA/cm^2 cell could be attributed to the presence of a resistive physical barrier that limits the access of the electrolyte to lithium metal. We note that the aged control cell and the 0.02 V cells have higher overpotentials (~0.11 V) than the unaged cell (0.08 V) suggesting that the aging process increases SEI thickness and charge-transfer impedance around the electrodeposited lithium, as has been previously reported.[25] We also use electrochemical impedance spectroscopy (EIS) to further understand the differences in SEI-mediated corrosion across our cells. SEI-mediated corrosion is characterized by the reaction of electrolytes with lithium, resulting in SEI growth.

https://doi.org/10.1021/acsenergylett.2c02137
ACS Energy Lett. 2023, 8, 869−877

This SEI growth is correlated with an increase in interfacial impedance,[36,37] making EIS an appropriate tool for investigating corrosion. In our EIS experiments, we deposit Li on Cu in a Li||Cu cell, then record interfacial impedance during the first 24 h of aging. Our EIS results show a 24-h impedance increase of 19%, 47.65%, and 56.43% for the 0.5 mA/cm^2, 0.02 V, and control cells, respectively (Figure 4C). This finding suggests that SEI-mediated corrosion is most reduced in the 0.5 mA/cm^2 cell, further supporting the improvements in CE for the 0.5 mA/cm^2 cell shown in Figure 4A. More details on the interfacial resistance calculations and Nyquist plots can be found in Supplementary Note 1 and Figure S14. All these results suggest that SEI formation is beneficial for improving performance in LMBs.

In this work, we develop constant current and constant voltage protocols for preforming an SEI in a high-performing electrolyte (1 M LiFSI/FDMB) and examine how the SEI impacts Coulombic efficiency and corrosion losses in LMBs. We reveal that SEI formation protocols can improve first-cycle CE by ∼5%, improve compounded CE in the first 5 electrochemical cycles by ∼7%, and reduce corrosion-induced CE losses by ∼8%. Constant voltage formation protocols carried out at 0.02 V vs Li$^+$/Li and constant current formation protocols carried out at 0.5 mA/cm^2 result in the best passivating SEIs for mitigating lithium−electrolyte reactions, especially in the first electrochemical cycle. We also show that constant current SEIs are more effective than constant voltage SEIs for improving performance, possibly because they are thicker and less permeable to electrolytes, resulting in reduced lithium−electrolyte reactions. Subsequently, we demonstrate that constant current SEIs reduce corrosion losses after 24 h of aging by maintaining a CE of 94.52%. In sum, this work shows that the SEI can be significantly optimized without changing electrolytes, thereby opening new pathways for electrolyte optimization in LMBs.

METHODS

Materials. The electrolyte used in this study (1 M LiFSI in FDMB solvent) was prepared and handled in an Ar-filled glovebox in which O_2 concentration was below 0.2 ppm and H_2O concentration was below 0.01 ppm. The FDMB solvent was synthesized as follows: Using a 1000 mL round-bottom flask, 400 mL of anhydrous tetrahydrofuran and 64 g of 2,2,3,3-tetrafluoro-1,4-butanediol were mixed, cooled to 0 °C, and stirred for 10 min. Subsequently, 40 g of NaH (60% in mineral oil) was added in batches and stirred at 0 °C for 30 min. Afterward, 140 g of methyl iodide was added slowly to the stirring suspension, and the ice bath was removed to enable the suspension warm up to room temperature. After stirring for 2 h at room temperature, the round-bottom flask was slowly heated to 60 °C to reflux overnight. After reaction completion, the flask was cooled down to room temperature, the mixture was filtered, and solvents were removed under vacuum. The crude product was distilled under vacuum (∼45 °C under 1 kPa) three times to yield a final, colorless liquid product. The FDMB electrolyte was prepared using 1 M LiFSI (Oakwood) in the FDMB solvent. High-purity Li foil (0.75 mm, 99.9% Alfa Aesar), Cu foil (Pred Materials), and polymer separator (Celgard 2325) were used to make cells in Li||Cu configurations for electrochemical tests, microscopy tests, and spectroscopy tests.

Electrochemistry. Type 2032 coin cells were assembled in an argon glovebox with a polymer separator (Celgard 2325). Li metal foil (0.75 mm thick, 99.9% Alfa Aesar) was used as the counter/reference electrode, and a Cu foil was used as the working electrode. Li was mechanically sheared to remove surface oxides and improve electrical contact, while Cu foil was rinsed with acetone, isopropyl alcohol, and deionized water to remove surface contaminants prior to cell assembly. The Li||Cu configuration was used for cyclability, SEM, and XPS characterizations. All Li||Cu cells were cycled at 25 °C on an Arbin battery cycler using the corresponding Li deposition current densities stated in the main text, and Li stripping was performed with a cutoff voltage of 1 V vs Li$^+$/Li. 30 μL of electrolyte was used in each instance where Li||Cu cells were cycled for CE and overpotential measurements. Li||Cu cells were used for EIS measurements after Li deposition on Cu under the current density conditions listed in the main text; 60 μL of electrolyte was used for aging and impedance experiments. The initial impedance measurements were carried out 5 min after lithium deposition, and impedance was continuously measured for 24 h after the initial measurements. Impedance measurements were carried out under open-circuit conditions within a frequency range of 1 MHz to 100 mHz, with a perturbation amplitude of 5 mV, using a Biologic VMP3 potentiostat.

Microscopy. All Li||Cu cells containing microscopy samples were dissembled inside an Ar glovebox immediately after electrochemical processes were completed. Subsequently, the Cu working electrodes containing the microscopy samples (lithium or SEI) were rinsed with fluorinated 1,4-dimethoxylbutane and dried inside the Ar glovebox before microscopy. All dried samples were transferred from the glovebox in an air-free vessel, with very minimal air exposure before the samples were introduced into the SEM tool. SEM and energy-dispersive X-ray spectroscopy mapping were performed using an FEI Magellan 400 XHR.

XPS Characterization. After lithium deposition and stripping cycles or SEI formation on Cu foil working electrodes, the electrodes were prepared in an Ar glovebox and rinsed with 90 μL of fluorinated 1,4-dimethoxylbutane to remove residual Li salts, then transferred to an XPS chamber using a vacuum transfer vessel. XPS signals were collected on a PHI VersaProbe 1 scanning XPS microprobe with an Al Kα source, and elemental spectra were shifted with reference to a C 1s binding energy of 284.6 eV.

ASSOCIATED CONTENT

Supporting Information

The Supporting Information is available free of charge at https://pubs.acs.org/doi/10.1021/acsenergylett.2c02137.

Supplementary Figures S1−S14, showing XPS spectra, coulometry measurements, SEM-EDS images, and impedance results (PDF)

AUTHOR INFORMATION

Corresponding Authors

Yi Cui − *Department of Materials Science and Engineering and Department of Energy Science and Engineering, Stanford University, Stanford, California 94305, United States; Stanford Institute for Materials and Energy Sciences, SLAC National Accelerator Laboratory, Menlo Park, California 94025, United States;* orcid.org/0000-0002-6103-6352; Email: yicui@stanford.edu

https://doi.org/10.1021/acsenergylett.2c02137
ACS Energy Lett. 2023, 8, 869−877

Stacey F. Bent − *Department of Chemical Engineering and Department of Energy Science and Engineering, Stanford University, Stanford, California 94305, United States;* orcid.org/0000-0002-1084-5336; Email: sbent@stanford.edu

Authors

Solomon T. Oyakhire − *Department of Chemical Engineering, Stanford University, Stanford, California 94305, United States;* orcid.org/0000-0002-3189-5949

Wenbo Zhang − *Department of Materials Science and Engineering, Stanford University, Stanford, California 94305, United States*

Zhiao Yu − *Department of Chemistry, Stanford University, Stanford, California 94305, United States;* orcid.org/0000-0001-8746-1640

Sarah E. Holmes − *Department of Chemistry, Stanford University, Stanford, California 94305, United States;* orcid.org/0000-0002-7946-964X

Philaphon Sayavong − *Department of Chemistry, Stanford University, Stanford, California 94305, United States*

Sang Cheol Kim − *Department of Materials Science and Engineering, Stanford University, Stanford, California 94305, United States;* orcid.org/0000-0002-1749-8277

David T. Boyle − *Department of Chemistry, Stanford University, Stanford, California 94305, United States;* orcid.org/0000-0002-0452-275X

Mun Sek Kim − *Department of Chemical Engineering and Department of Materials Science and Engineering, Stanford University, Stanford, California 94305, United States*

Zewen Zhang − *Department of Materials Science and Engineering, Stanford University, Stanford, California 94305, United States;* orcid.org/0000-0002-4909-4330

Complete contact information is available at: https://pubs.acs.org/10.1021/acsenergylett.2c02137

Author Contributions

S.T.O., Y.C., and S.F.B. conceived the idea and designed the experiments. S.T.O. carried out electrochemical tests and XPS experiments. S.E.H. assisted with electrochemical experiments. W.Z. and P.S. carried out all SEM experiments. Z.Y. synthesized and provided FDMB electrolyte. S.C.K., D.T.B., M.S.K., and Z.Z. provided helpful discussions and assisted with interpretation of results. S.T.O., Y.C., and S.F.B. wrote the manuscript. All authors discussed and commented on the manuscript.

Notes

The authors declare no competing financial interest.

■ ACKNOWLEDGMENTS

S.T.O. acknowledges support from the Knight-Hennessy scholarship for graduate studies at Stanford University and the TomKat Center Fellowship for Translational Research at Stanford University. Z.Z. acknowledges support from the Stanford Interdisciplinary Graduate Fellowship. Y.C. acknowledges support from the Assistant Secretary for Energy, Efficiency and Renewable Energy, Office of Vehicle Technologies, of the U.S. Department of Energy under the Battery Materials Research (BMR) Program and the Battery500 Consortium program. Part of this work was performed at the Stanford Nano Shared Facilities (SNSF), supported by the National Science Foundation under award ECCS-2026822.

■ REFERENCES

(1) Agre, P.; Molina, M.; Chu, S. The Real Climate Debate. *Nature* **2017**, *550* (7675), S62−S64.

(2) Liu, J.; Bao, Z.; Cui, Y.; Dufek, E. J.; Goodenough, J. B.; Khalifah, P.; Li, Q.; Liaw, B. Y.; Liu, P.; Manthiram, A.; Meng, Y. S.; Subramanian, V. R.; Toney, M. F.; Viswanathan, V. V.; Whittingham, M. S.; Xiao, J.; Xu, W.; Yang, J.; Yang, X.-Q.; Zhang, J.-G. Pathways for Practical High-Energy Long-Cycling Lithium Metal Batteries. *Nat. Energy* **2019**, *4* (3), 180−186.

(3) Lin, D.; Liu, Y.; Cui, Y. Reviving the Lithium Metal Anode for High-Energy Batteries. *Nat. Nanotechnol.* **2017**, *12* (3), 194−206.

(4) Wang, H.; Liu, Y.; Li, Y.; Cui, Y. Lithium Metal Anode Materials Design: Interphase and Host. *Electrochem. Energy Rev,* **2019**, *2* (4), 509−517.

(5) Yu, Z.; Cui, Y.; Bao, Z. Design Principles of Artificial Solid Electrolyte Interphases for Lithium-Metal Anodes. *Cell Reports Phys. Sci.* **2020**, *1* (7), 100119.

(6) Niu, C.; Liu, D.; Lochala, J. A.; Anderson, C. S.; Cao, X.; Gross, M. E.; Xu, W.; Zhang, J.-G.; Whittingham, M. S.; Xiao, J.; Liu, J. Balancing Interfacial Reactions to Achieve Long Cycle Life in High-Energy Lithium Metal Batteries. *Nat. Energy* **2021**, *6* (7), 723−732.

(7) Yu, Z.; Wang, H.; Kong, X.; Huang, W.; Tsao, Y.; Mackanic, D. G.; Wang, K.; Wang, X.; Huang, W.; Choudhury, S.; Zheng, Y.; Amanchukwu, C. V.; Hung, S. T.; Ma, Y.; Lomeli, E. G.; Qin, J.; Cui, Y.; Bao, Z. Molecular Design for Electrolyte Solvents Enabling Energy-Dense and Long-Cycling Lithium Metal Batteries. *Nat. Energy* **2020**, *5* (7), 526−533.

(8) Lee, S. H.; Hwang, J.-Y.; Ming, J.; Kim, H.; Jung, H.-G.; Sun, Y.-K. Long-Lasting Solid Electrolyte Interphase for Stable Li-Metal Batteries. *ACS Energy Lett.* **2021**, *6* (6), 2153−2161.

(9) Louli, A. J.; Eldesoky, A.; Weber, R.; Genovese, M.; Coon, M.; deGooyer, J.; Deng, Z.; White, R. T.; Lee, J.; Rodgers, T.; Petibon, R.; Hy, S.; Cheng, S. J. H.; Dahn, J. R. Diagnosing and Correcting Anode-Free Cell Failure via Electrolyte and Morphological Analysis. *Nat. Energy* **2020**, *5* (9), 693−702.

(10) Amanchukwu, C. V.; Yu, Z.; Kong, X.; Qin, J.; Cui, Y.; Bao, Z. A New Class of Ionically Conducting Fluorinated Ether Electrolytes with High Electrochemical Stability. *J. Am. Chem. Soc.* **2020**, *142* (16), 7393−7403.

(11) Xue, W.; Huang, M.; Li, Y.; Zhu, Y. G.; Gao, R.; Xiao, X.; Zhang, W.; Li, S.; Xu, G.; Yu, Y.; Li, P.; Lopez, J.; Yu, D.; Dong, Y.; Fan, W.; Shi, Z.; Xiong, R.; Sun, C.-J.; Hwang, I.; Lee, W.-K.; Shao-Horn, Y.; Johnson, J. A.; Li, J. Ultra-High-Voltage Ni-Rich Layered Cathodes in Practical Li Metal Batteries Enabled by a Sulfonamide-Based Electrolyte. *Nat. Energy* **2021**, *6* (5), 495−505.

(12) Ugata, Y.; Tatara, R.; Mandai, T.; Ueno, K.; Watanabe, M.; Dokko, K. Understanding the Reductive Decomposition of Highly Concentrated Li Salt/Sulfolane Electrolytes during Li Deposition and Dissolution. *ACS Appl. Energy Mater.* **2021**, *4* (2), 1851−1859.

(13) Kang, D. W.; Moon, J.; Choi, H. Y.; Shin, H. C.; Kim, B. G. Stable Cycling and Uniform Lithium Deposition in Anode-Free Lithium-Metal Batteries Enabled by a High-Concentration Dual-Salt Electrolyte with High $LiNO_3$ Content. *J. Power Sources* **2021**, *490*, 229504.

(14) Shi, P.; Zhang, L.; Xiang, H.; Liang, X.; Sun, Y.; Xu, W. Lithium Difluorophosphate as a Dendrite-Suppressing Additive for Lithium Metal Batteries. *ACS Appl. Mater. Interfaces* **2018**, *10* (26), 22201−22209.

(15) Li, W.; Yao, H.; Yan, K.; Zheng, G.; Liang, Z.; Chiang, Y.-M.; Cui, Y. The Synergetic Effect of Lithium Polysulfide and Lithium Nitrate to Prevent Lithium Dendrite Growth. *Nat. Commun.* **2015**, *6* (1), 1−8.

(16) Wang, H.; Yu, Z.; Kong, X.; Huang, W.; Zhang, Z.; Mackanic, D. G.; Huang, X.; Qin, J.; Bao, Z.; Cui, Y. Dual-Solvent Li-Ion Solvation Enables High-Performance Li-Metal Batteries. *Adv. Mater.* **2021**, *33* (25), 2008619.

(17) Weber, R.; Genovese, M.; Louli, A. J.; Hames, S.; Martin, C.; Hill, I. G.; Dahn, J. R. Long Cycle Life and Dendrite-Free Lithium

Morphology in Anode-Free Lithium Pouch Cells Enabled by a Dual-Salt Liquid Electrolyte. *Nat. Energy* **2019**, *4* (8), 683−689.
(18) Yamada, Y.; Wang, J.; Ko, S.; Watanabe, E.; Yamada, A. Advances and Issues in Developing Salt-Concentrated Battery Electrolytes. *Nat. Energy* **2019**, *4* (4), 269−280.
(19) Kim, S. C.; Kong, X.; Vilá, R. A.; Huang, W.; Chen, Y.; Boyle, D. T.; Yu, Z.; Wang, H.; Bao, Z.; Qin, J.; Cui, Y. Potentiometric Measurement to Probe Solvation Energy and Its Correlation to Lithium Battery Cyclability. *J. Am. Chem. Soc.* **2021**, *143* (27), 10301−10308.
(20) Yao, Y.-X.; Chen, X.; Yan, C.; Zhang, X.-Q.; Cai, W.-L.; Huang, J.-Q.; Zhang, Q. Regulating Interfacial Chemistry in Lithium-Ion Batteries by a Weakly Solvating Electrolyte**. *Angew. Chem., Int. Ed.* **2021**, *60* (8), 4090−4097.
(21) Ren, X.; Zou, L.; Cao, X.; Engelhard, M. H.; Liu, W.; Burton, S. D.; Lee, H.; Niu, C.; Matthews, B. E.; Zhu, Z.; Wang, C.; Arey, B. W.; Xiao, J.; Liu, J.; Zhang, J. G.; Xu, W. Enabling High-Voltage Lithium-Metal Batteries under Practical Conditions. *Joule* **2019**, *3* (7), 1662−1676.
(22) Cao, X.; Jia, H.; Xu, W.; Zhang, J.-G. Review—Localized High-Concentration Electrolytes for Lithium Batteries. *J. Electrochem. Soc.* **2021**, *168* (1), 010522.
(23) Kolesnikov, A.; Kolek, M.; Dohmann, J. F.; Horsthemke, F.; Börner, M.; Bieker, P.; Winter, M.; Stan, M. C. Galvanic Corrosion of Lithium-Powder-Based Electrodes. *Adv. Energy Mater.* **2020**, *10* (15), 2000017.
(24) Lin, D.; Liu, Y.; Li, Y.; Li, Y.; Pei, A.; Xie, J.; Huang, W.; Cui, Y. Fast Galvanic Lithium Corrosion Involving a Kirkendall-Type Mechanism. *Nat. Chem.* **2019**, *11* (4), 382−389.
(25) Boyle, D. T.; Huang, W.; Wang, H.; Li, Y.; Chen, H.; Yu, Z.; Zhang, W.; Bao, Z.; Cui, Y. Corrosion of Lithium Metal Anodes during Calendar Ageing and Its Microscopic Origins. *Nat. Energy* **2021**, *6* (5), 487−494.
(26) Menkin, S.; O'Keefe, C. A.; Gunnarsdóttir, A. B.; Dey, S.; Pesci, F. M.; Shen, Z.; Aguadero, A.; Grey, C. P. Toward an Understanding of SEI Formation and Lithium Plating on Copper in Anode-Free Batteries. *J. Phys. Chem. C* **2021**, *125* (30), 16719−16732.
(27) Huang, W.; Boyle, D. T.; Li, Y.; Li, Y.; Pei, A.; Chen, H.; Cui, Y. Nanostructural and Electrochemical Evolution of the Solid-Electrolyte Interphase on CuO Nanowires Revealed by Cryogenic-Electron Microscopy and Impedance Spectroscopy. *ACS Nano* **2019**, *13* (1), 737−744.
(28) Xu, Y.; Wu, H.; Jia, H.; Engelhard, M. H.; Zhang, J. G.; Xu, W.; Wang, C. Sweeping Potential Regulated Structural and Chemical Evolution of Solid-Electrolyte Interphase on Cu and Li as Revealed by Cryo-TEM. *Nano Energy* **2020**, *76*, 105040.
(29) Oyakhire, S. T.; Gong, H.; Cui, Y.; Bao, Z.; Bent, S. F. An X-Ray Photoelectron Spectroscopy Primer for Solid Electrolyte Interphase Characterization in Lithium Metal Anodes. *ACS Energy Lett.* **2022**, *7* (8), 2540−2546.
(30) Xiang, Y.; Tao, M.; Zhong, G.; Liang, Z.; Zheng, G.; Huang, X.; Liu, X.; Jin, Y.; Xu, N.; Armand, M.; Zhang, J.-G.; Xu, K.; Fu, R.; Yang, Y. Quantitatively Analyzing the Failure Processes of Rechargeable Li Metal Batteries. *Sci. Adv.* **2021**, *7* (46), eabj3423.
(31) Gunnarsdóttir, A. B.; Amanchukwu, C. V.; Menkin, S.; Grey, C. P. Noninvasive In Situ NMR Study of "Dead Lithium" Formation and Lithium Corrosion in Full-Cell Lithium Metal Batteries. *J. Am. Chem. Soc.* **2020**, *142* (49), 20814−20827.
(32) Oyakhire, S. T.; Huang, W.; Wang, H.; Boyle, D. T.; Schneider, J. R.; Paula, C.; Wu, Y.; Cui, Y.; Bent, S. F. Revealing and Elucidating ALD-Derived Control of Lithium Plating Microstructure. *Adv. Energy Mater.* **2020**, *10*, 2002736.
(33) Oyakhire, S. T.; Zhang, W.; Shin, A.; Xu, R.; Boyle, D. T.; Yu, Z.; Ye, Y.; Yang, Y.; Raiford, J. A.; Huang, W.; Schneider, J. R.; Cui, Y.; Bent, S. F. Electrical Resistance of the Current Collector Controls Lithium Morphology. *Nat. Commun.* **2022**, *13* (1), 1−12.
(34) Shin, W.; Manthiram, A. A Facile Potential Hold Method for Fostering an Inorganic Solid-Electrolyte Interphase for Anode-Free Lithium-Metal Batteries. *Angew. Chem., Int. Ed.* **2022**, *61* (13), 202115909 DOI: 10.1002/anie.202115909.
(35) Wang, H.; Huang, W.; Yu, Z.; Huang, W.; Xu, R.; Zhang, Z.; Bao, Z.; Cui, Y. Efficient Lithium Metal Cycling over a Wide Range of Pressures from an Anion-Derived Solid-Electrolyte Interphase Framework. *ACS Energy Lett.* **2021**, *6* (2), 816−825.
(36) Wood, S. M.; Fang, C.; Dufek, E. J.; Nagpure, S. C.; Sazhin, S. V.; Liaw, B.; Meng, Y. S. Predicting Calendar Aging in Lithium Metal Secondary Batteries: The Impacts of Solid Electrolyte Interphase Composition and Stability. *Adv. Energy Mater.* **2018**, *8* (26), 1801427.
(37) Peled, E.; Menkin, S. Review—SEI: Past, Present and Future. *J. Electrochem. Soc.* **2017**, *164* (7), A1703−A1719.

https://doi.org/10.1021/acsenergylett.2c02137
ACS Energy Lett. 2023, 8, 869−877